PCCP

PAPER

View Article Online
View Journal | View Issue

Cite this: *Phys. Chem. Chem. Phys.*, 2015, **17**, 18677

Metal containing cryptands as hosts for anions: evaluation of Cu(I)···X and π···X interactions in halide–tricopper(I) complexes through relativistic DFT calculations†

Miguel Ponce-Vargas*[a] and Alvaro Muñoz-Castro*[b]

Received 12th May 2015,
Accepted 11th June 2015

DOI: 10.1039/c5cp02737c

www.rsc.org/pccp

More selective than crown ethers, cryptands arise as suitable hosts for several ions, with the size of the cavity and the behavior of the atoms belonging to the structure being the main factors governing their selectivity. Similar to metallacrowns, inorganic counterparts of crown ethers, the presence of metal centers in cryptands can offer significant advantages in terms of ion recognition as they provide positively charged sites, which allow them to encapsulate anions. Here, through density functional methodologies, we evaluate the preference of a tricopper(I) cryptand host toward a series of halide ions ranging from the hard fluoride to the soft iodide, where the more intense interactions are established with the hardest one, and the electrostatic term is the more relevant contributor to total interaction energy. Upon exploration of this electrostatic contribution in more detail, it is observed that as the guest becomes softer, the increase of higher order Coulombic terms, such as dipole–dipole, dipole–quadrupole, and quadrupole–quadrupole, acquires more relevance on going from 9.22% to 41.25%, denoting the key role and variation of such forces in inclusion systems with metal-containing hosts.

Introduction

Designed to be three-dimensional complements to crown ethers, cryptands are structures particularly prominent as specific sequestering agents,[1–4] with larger binding affinities than those corresponding to crown ethers.[5] Due to their three-dimensional spatial structures and additional binding sites they possess enhanced selectivity[6] and stimuli-responsiveness[7] properties.

Cryptands can also be used as phase-transfer catalysts[8] and solid electrolytes.[9] In addition, they have been recently tested as fluorescent sensors for radioactive pertechnetate anions with very promising results.[10] For such structures, the inclusion of a heteroatom in a host cavity can tune their recognition capabilities,[11,12] similar to metallacrowns – inorganic counterparts of crown ethers – in which the inclusion of metal centers confer them unique host–guest properties. Then, it is expected that the incorporation of metal centers in cryptands[11] will alter the nature of the interactions responsible for keeping the guest species enclosed. In this context, the tricopper cluster housed within a tris(β-diketimine) cyclophane ligand, Cu_3L (L = β-diketiminate), recently synthesized by Di Francesco and coworkers, provides us a very interesting study case,[13] as it possesses three copper(I) centers capable of interacting simultaneously with a halide ion, leading to a $[Cu_3LCl]^-$ complex, in which Cu(I)···X interactions arise as the driving forces of the host–guest coupling. This inclusion system constitutes an interesting case, due to the fact that most cryptand receptors interact with anions *via* hydrogen bonds,[14] leading to an ideal starting point for the evaluation of the preference of the soft acid Cu(I), according to the Hard and Soft Acid and Bases (HSAB) Principle,[15,16] toward a series of halide guests on going from the hard fluoride to the soft iodide.

As host–guest interactions involving ions exhibit mainly an electrostatic character,[17,18] the use of electric multipole moments seems to be a reasonable way for the evaluation of the electronic cloud departure experienced at the binding sites, which is closely related to non-covalent forces.[19] In the same line, by using multipole moment tensors, several phenomena such as solid-state architectures of aromatic molecules,[20] π···π interactions in benzene dimers,[21] noncovalent forces between amino acids and aromatic groups,[22] and solvation of aromatic compounds by ionic liquids[23] can been clearly explained. Additionally, the driving forces in the design of supramolecular assemblies have been modeled through ion-multipole interactions.[24]

As part of our current interest in noncovalent interactions involving host species with metal centers acting as binding sites,[25,26] here we extend our efforts to systems involving both

[a] *Institut des Sciences Chimiques de Rennes UMR 6226, Université de Rennes 1, Campus de Beaulieu, 35042 Rennes, France. E-mail: miguel-armando.ponce-vargas@univ-rennes1.fr*
[b] *Dirección de Postgrado e Investigación, Universidad Autónoma de Chile, Carlos Antúnez 1920, Santiago, Chile. E-mail: alvaro.munoz@uautonoma.cl*

† Electronic supplementary information (ESI) available. See DOI: 10.1039/c5cp02737c

metal$\cdots X^-$ and $\pi\cdots X^-$ interactions for the evaluation of the nature of the host–guest formation in terms of such types of interactions towards the formation of the overall complex.

The nature of the host–guest interactions was evaluated according to the Ziegler–Morokuma energy partitioning scheme,[27,28] including the dispersion term in line with the pairwise Grimme approach,[29,30] while the multipole analysis at the binding sites and guest species is carried out according to the Swart methodology.[31] Also the graphical representation of the multipole moment tensors is presented in order to relate it with the electronic cloud departure experienced by the copper centers with the guest arrival. Finally, the spatial representation of the interactions involved in the formation of the host–guest pair is obtained according to the non-covalent interaction (NCI) analysis proposed by Yang and coworkers, which allows a topological study of the noncovalent interactions.[32,33]

Computational details

Relativistic density functional theory calculations[34] were carried out by using the ADF 2012.02 code,[35] *via* the scalar ZORA Hamiltonian, in order to account for relativistic effects. Triple-ξ Slater basis set plus a polarization function (STO-TZP) in conjunction to the meta-generalized gradient approximation of Tao, Perdew, Staroverov, and Scuseria (TPSS)[36] has been employed. In addition to the density $\rho(r)$, and its gradient $\nabla\rho(r)$, the meta-GGA functionals also use information extracted from the orbital-dependent kinetic energy density $1/2\sum|\nabla\varphi^{KS}(r)|^2$ (where φ^{KS} represents the Kohn–Sham orbitals). This added flexibility in the functional form allows for a more complete satisfaction of properties of the elusive true density functional, compared to GGA functionals.[37] The performance of the TPSS functional has been evaluated in the description of hydrogen-bonded complexes,[38] binding energies of 3d-transition metal dimers,[39] and low-lying excitation energies of small molecules and atoms.[40] Geometry optimizations were done *via* the analytical energy gradient method implemented by Verluis and Ziegler.[41] In order to consider long-range interactions, the dispersion Grimme correction is added both for geometry optimizations and energy decomposition analysis.

The local multipole moment calculation is conducted in three stages according to the method developed by Swart *et al.*,[31] in which at the first step, the molecular charge density is expressed as a sum of atomic densities. Then, a set of atomic multipoles is defined from such atomic densities and used to obtain the electrostatic potential outside the charge distribution. Finally, to keep the atomic multipoles as local as possible, a weight function that falls off rapidly is used.

The graphical representation of the quadrupole tensors (Θ) was obtained based on the method employed by Autschbach and coworkers,[42] considering a function written in spherical coordinates representing the $f(r) = \sum_{ij} r_i r_j \Theta_{ij}$ expression centered at the respective nucleus, depicting its angular dependence and sign. The non-covalent interaction (NCI) analysis was carried out by using the NCIPLOT program developed by Weitao Yang and coworkers,[32,33] based on the analysis of electron density descriptors. All isosurfaces and figures have been drawn by using the software packages Chemcraft[43] and Visual Molecular Dynamics (VMD).[44]

Results and discussion

Both, cryptand host (**1**) and its chloride complex (**1**-Cl) belong to the D_{3h} symmetry group, where the copper centers are arranged in a triangular conformation around the halide guest (Scheme 1). Here, we extend this study to the F^-, Br^-, and I^- derivatives in order to gain a better understanding of the host–guest coupling. The cryptand host is obtained from the reaction of benzyl potassium, THF, and CuBr, whereas the chloride inclusion system is generated by a similar procedure, but this time adding CuCl as the copper source. As is observed in Table 1, the Cu–Cu distance decreases with the guest entry from 4.280 Å to an average value of 3.956 Å, evidencing the interaction of the copper centers with the guest species. Also, such a distance varies in line with the guest size on going from 3.654 Å (**1**-F) to 4.232 Å (**1**-I) denoting high stabilizing interactions between the copper centers and the guest ion in **1**-F. The same trend is observed with the Cu$\cdots$center distance, which ranges from 2.109 Å (**1**-F) to 2.443 Å (**1**-I) showing the ability of the cavity to adjust its size according to the guest. The N–Cu–N angle increases as the Cu$\cdots$X lengthens, whereas the $C_6\cdots X$ distance remains almost unaltered along the series, suggesting that Cu(I) centers mainly define the cavity size (see Fig. 1).

The Energy Decomposition Analysis (EDA) proposed by Morokuma provides insights into intermolecular interactions by decomposing the total interaction energy into various terms of chemical relevance such as electrostatic and Pauli repulsion, and orbital overlapping.[27,28,45] The interaction between the frozen charge densities of the host and the guest at the equilibrium geometry of the inclusion compound is accounted by the electrostatic interaction ΔE_{elec}, which is calculated by subtracting the Coulomb integral of the fragments from that corresponding to the overall system. This term is particularly useful to qualitatively explain and evaluate many structural and energetic features related to non-covalent systems.[46]

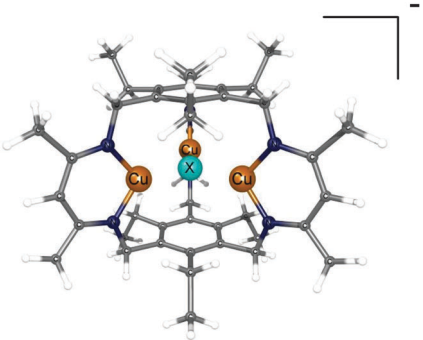

Scheme 1 Structure for **1**-X (X = F, Cl, Br, I).

Table 1 Selected distances (Å) and angles (degrees) of the host and halide complexes

	1	1-F	1-Cl		1-Br	1-I
	Calc.	Calc.	Exp.[a]	Calc.	Calc.	Calc.
Cu–Cu	4.280	3.654	3.785	3.894	4.044	4.232
Cu···X	—	2.109	2.186	2.248	2.335	2.443
N–Cu	1.842	1.950	1.938	1.914	1.894	1.874
N–N	3.177	3.035	3.064	3.081	3.115	3.160
C_6···X	—	3.022	3.036	3.043	3.057	3.083
∠N–Cu–N	119.2°	102.2°	104.5°	107.2°	110.7°	115.0°

[a] Structural parameters from ref. 13.

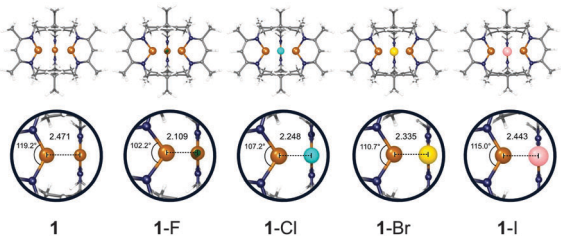

Fig. 1 Some relevant structural parameters of the host and inclusion systems. In **1**, the distance is measured between one of the Cu(I) and the center of the cavity.

The product of density fragments is antisymmetrized and renormalized to give an intermediate state. The energy difference between the states before and after antisymmetrization and renormalization is termed as Pauli repulsion, ΔE_{Pauli}, and can be related to destabilizing forces between the fragments. Finally, the fragment orbitals are relaxed to yield the final state corresponding to the inclusion system. The decrease in energy due to such orbital mixing is identified as the orbital interaction, ΔE_{orb}. By adding ΔE_{elec}, ΔE_{Pauli}, and ΔE_{orb} we obtain the total interaction energy ΔE_{int} of the fragments.[47] To overcome the basis set superposition error (BSSE), the counterpoise method proposed by Boys and Bernardi is employed denoting a BSSE value of about 4.8 kcal mol^{-1}.[48] The dispersion interaction is included according to the Grimme pairwise dispersion correction where an attractive energy term summed over all atomic pairs is incorporated.[29,30] It takes into account the weak forces associated with instantaneous fluctuations of fragment electronic densities.

The energy difference between the initial geometries of the moieties and those corresponding to the fragments being part of the inclusion systems is denoted as preparation energy, ΔE_{prep}. It is related to the host structural variation with the guest entry, which is not taken into account in order to describe the nature of the host–guest interaction energy (ΔE_{int}). In the halide series, which is the subject of this study, ΔE_{prep} is about 11.51 kcal mol^{-1} (Table 2) evidencing the structural changes upon the guest entry, which are mainly associated with the displacements of the copper centers, as mentioned above.

The EDA (Table 2) shows that total interaction energy (ΔE_{int}) becomes more stabilizing as the guest becomes softer, ranging from −90.05 kcal mol^{-1} in **1**-F to −41.55 kcal mol^{-1} for **1**-I, denoting the stronger host–guest interactions occurring in **1**-F. Such preference for the hardest guest can be attributed to the marked decrease of the Pauli repulsion term (ΔE_{Pauli}), which accounts for the steric repulsion, as the guest becomes smaller, being 385.86 (**1**-I) > 309.88 (**1**-Br) > 262.95 (**1**-Cl), and 125.54 kcal mol^{-1} in **1**-F, in agreement to the increase of their ionic radii.[49] Within the stabilizing terms, the Coulombic term (ΔE_{elec}) arises as the most important contributor to ΔE_{int} representing about 74%, followed by the orbital term (ΔE_{orb}) of about 23%, and dispersion forces (ΔE_{disp}) of 2.70%.

The electrostatic term is more favorable as the guest becomes softer ranging from −146.69 kcal mol^{-1} in **1**-F to −331.55 kcal mol^{-1} for **1**-I, suggesting that higher-rank electrostatic terms such as dipole–quadrupole and quadrupole–quadrupole forces acquire more relevance as the halide ion becomes larger.[25] The same trend is observed with the orbital contribution, which can be associated with the host and guest orbitals overlap, varying from −65.67 kcal mol^{-1} to −81.76 kcal mol^{-1}, in line with the more effective charge transfer occurring in **1**-I (*vide infra*). The dispersion term associated with instantaneous electronic cloud fluctuations varies from −3.23 kcal mol^{-1} in **1**-F to −14.10 kcal mol^{-1} in **1**-I, in good agreement with the higher electronic cloud departure experienced by the iodide guest.

In order to gain a deeper understanding of the more relevant term of the host–guest interaction, namely ΔE_{elec}, we split this term into two main Coulombic contributions, one that encompasses all ion-multipole forces (ion–dipole, ion–quadrupole, *etc.*) related to the anionic character of the guest, and another concerning higher order interactions (dipole–dipole, dipole–quadrupole,

Table 2 Energy Decomposition Analysis (EDA) (kcal mol^{-1}) and Natural Population Analysis (NPA) (a.u.) of the host and halide complexes

	1	1-F		1-Cl		1-Br		1-I	
EDA									
ΔE_{prep}	—	16.95		11.53		9.29		8.28	
ΔE_{orb}	—	−65.67	30.46%	−79.35	23.57%	−76.49	20.74%	−81.76	19.13%
ΔE_{elec}	—	−146.69	68.04%	−247.99	73.65%	−280.52	76.04%	−331.55	77.57%
ΔE_{disp}	—	−3.23	1.50%	−9.36	2.78%	−11.88	3.22%	−14.10	3.30%
ΔE_{Pauli}	—	125.54		262.95		309.88		385.86	
ΔE_{int}	—	−90.05		−73.75		−59.01		−41.55	
NPA									
X	—	−0.85		−0.71		−0.66		−0.43	
[Cu_3]	2.60	2.82		2.66		2.62		2.38	
2[C_6]	−0.04	0.00		0.03		0.04		0.06	
[$C_{45}H_{63}N_6$]	−2.60	−2.97		−2.95		−2.96		−2.95	

quadrupole–quadrupole, *etc.*), which depends on the guest nature according to the HSAB theory.[25,26] Thus, we replaced the halide ions by the corresponding noble gases, in such a way that all ion-multipole terms are cancelled, leaving only the terms related to higher-rank Coulombic interactions. Once this replacement is carried out, a sharp decline of the electrostatic contribution can be observed, which now ranges from −13.53 kcal mol^{-1} to −136.75 kcal mol^{-1} on going from **1**-Ne to **1**-Xe, significantly lower in comparison to the halide series. Hence, the electrostatic contribution of higher order Coulombic terms can be estimated by the expression $(1 - {}^{Ng}\Delta E_{elec}/{}^{X}\Delta E_{elec}) \times 100$, where ${}^{Ng}\Delta E_{elec}$ and ${}^{X}\Delta E_{elec}$ represent the electrostatic contributions of the noble gas and halide series, respectively.[25,26] Through the use of this approach it can be observed that as the guest becomes softer the higher-order terms acquire more relevance, on going from 9.22% in **1**-F to 41.25% in **1**-I, where the iodide guest is able to experience the higher electronic cloud distortion leading to an increased participation of such terms in the host–guest coupling.

With the aim to evaluate the relevance of Cu(I)···X and π···X forces, depicting the role of the copper centers and the aromatic rings of the cryptand structure (**1**) into the magnitude of the host–guest interactions, we carried out two independent energy decomposition analyses. One concerning the interactions between the guest species and the copper-containing arms (denoted as **2**), and another corresponding to the forces between the guest and the aromatic rings located above and below them (denoted as **3**) (Table 3). As a result, the major relevance of the former binding sites in the encapsulation of halide ions is clear, with total interaction energies ranging from −99.36 kcal mol^{-1} for **2**-F to −61.75 kcal mol^{-1} for **2**-I, larger than those arising between the aromatic rings and the guest species, which are even destabilizing for **3**-Br and **3**-I. These results also reflect mainly the electrostatic character of the interaction between the Cu(I) centers and the halide species, representing about 73% of the total interaction energy in **2**-X. On the other hand, dispersion forces contribute to a minor extent, becoming more relevant in the **3**-X series, reaching a value of −11.86 kcal mol^{-1} in **3**-I, where the iodide anion is closer to the π aromatic density.

The Natural Population Analysis allows the evaluation of the charge upon guest inclusion. As is observed in Table 2, each halide ion varies from its isolated −1.0 |*e*| charge to −0.85 |*e*| in **1**-F, −0.71 |*e*| (**1**-Cl), −0.66 |*e*| (**1**-Br) and −0.43 |*e*| in **1**-I, which depicts the iodide counterpart as the system where a more effective charge transfer occurs, in agreement to ΔE_{orb} (*vide intra*). Consequently, it can be concluded from the electronic configurations of the halide guests that the electronic density comes primarily from the np orbitals (Table 4). The charge distribution in the host cavity leads to a more positive charge located over the copper centers (+2.60 |*e*|), while the organic framework possesses a total charge of +1.46 |*e*|. With the guest entry the copper center charges now range from +2.82 |*e*| in **1**-F to +2.38 |*e*| in **1**-I, while the charge of the aromatic rings located above and below the guest species experiences the most important variation of about 0.5 |*e*| ranging from 0.95 |*e*| (**1**-F) to 1.00 |*e*| (**1**-I), suggesting that transferred density is stabilized mainly by resonance over the aromatic rings. Such electronic charge transfer from the halide ions to the organic groups is probably mediated by the copper centers, as the orbital contribution is more relevant in the **2**-X series (∼−86.54 kcal mol^{-1}) than in **3**-X (∼−15.45 kcal mol^{-1}). Interestingly a slight amount of charge transferred in **1**-I is retained in the copper centers (0.22 |*e*|), which could indicate that there exists a limit in the electronic density accepted by the organic framework.

The variation of the charge distribution at the Cu(II) binding sites accounts for the electrostatic nature of the interaction (ΔE_{elec}), which can be evaluated according to the atomic multipole expansion, a local property. The analysis derived from an atomic multipole expansion proposed by Swart and coworkers[31] offers an accurate description of the electrostatic potential given by the charge distribution in the whole molecule. This is achieved by writing the total density as a sum of atomic densities expressed in terms of atomic functions, and by defining a set of atomic multipoles from such atomic functions.

Table 4 Electronic configurations for representative copper centers and guest species

1	Cu $[Ar]4s^{0.39}3d^{9.74}$
1-F	Cu $[Ar]4s^{0.34}3d^{9.76}$
	F $[He]2s^{1.96}2p^{5.88}$
1-Cl	Cu $[Ar]4s^{0.34}3d^{9.76}$
	Cl $[Ne]3s^{1.91}3p^{5.87}$
1-Br	Cu $[Ar]4s^{0.35}3d^{9.76}$
	Br $[Ar]4s^{1.92}3d^{10.0}4p^{5.71}$
1-I	Cu $[Ar]4s^{0.43}3d^{9.75}$
	I $[Kr]5s^{1.76}4d^{10.0}5p^{5.63}$

Table 3 Energy Decomposition Analysis (EDA) (kcal mol^{-1}) for the arms (**2**) and rings (**3**) moieties

Arms	**2**-F		**2**-Cl		**2**-Br		**2**-I	
ΔE_{orb}	−80.49	34.48%	−92.13	26.21%	−86.60	23.14%	−86.87	20.92%
ΔE_{elec}	−151.65	64.96%	−255.18	72.59%	−282.10	75.37%	−321.17	77.33%
ΔE_{disp}	−1.30	0.56%	−4.24	1.21%	−5.58	1.49%	−7.26	1.75%
ΔE_{Pauli}	134.08		265.99		301.20		353.55	
ΔE_{int}	−99.36		−85.56		−73.08		−61.75	
Rings	**3**-F		**3**-Cl		**3**-Br		**3**-I	
ΔE_{orb}	−15.50	82.71%	−14.85	54.50%	−15.09	35.84%	−16.37	24.37%
ΔE_{elec}	8.49		−4.33	15.89%	−16.95	40.26%	−38.95	57.98%
ΔE_{disp}	−3.24	17.29%	−8.07	29.61%	−10.06	23.90%	−11.86	17.65%
ΔE_{Pauli}	7.06		27.00		45.30		76.70	
ΔE_{int}	−3.19		−0.25		3.20		9.52	

Table 5 Dipole moment magnitudes (D) of a representative copper center in the studied systems and the arm (**2**) moieties

	1	**1**-F	**1**-Cl	**1**-Br	**1**-I
1-X	0.0062	0.2235	0.0948	0.0356	0.4064
2-X	0.1675	0.1928	0.0874	0.0093	0.4002

The local dipole moment analysis (Table 5 and Fig. 2) for copper reveals that before the guest entry the dipole term is very low (0.0062 D) suggesting an almost spherical distribution of the respective electronic cloud. The guest entry produces a slight variation in the vector magnitude, being 0.2235 D in **1**-F, 0.0948 D in **1**-Cl, and 0.0356 D in **1**-Br. The maximum dipole variation occurs in the **1**-I case (0.4064 D), in line with the relevance of higher order terms in the electrostatic expansion aforementioned.

The dipole moment magnitudes obtained with other exchange correlation functionals present the same trend along the series (ESI†). Owing to symmetry considerations ruled by the D_{3h} point group of the studied systems, the halide guest exhibits no local dipole-moment ($\mu = 0$).

To obtain a deeper understanding of the contribution to the host–guest coupling from the quadrupole moment (Θ) at the binding sites, we evaluate the local quadrupole moment tensors in each copper center, and the guest species (Fig. 3).

Such tensors are considered under their principal axis system (PAS) where the principal components are denoted independent of the molecular system axis (Table 6), in the present work we define the Θ_{33} component as the largest absolute value. Such terms can be optionally designated according to $\Theta_{11} > \Theta_{22} > \Theta_{33}$, depicting the more negative component as Θ_{33}, such an approach leads to similar conclusions (ESI†). The departure from the spherical symmetry of the quadrupole moment can be quantified through the quadrupole anisotropic component (Θ_{aniso}), in analogy to the Haeberlen convention from solid-state NMR[50] resulting in a single parameter, which clearly accounts for such distortion.

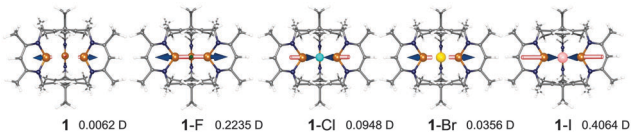

Fig. 2 Graphical representation of the copper dipole moment vectors.

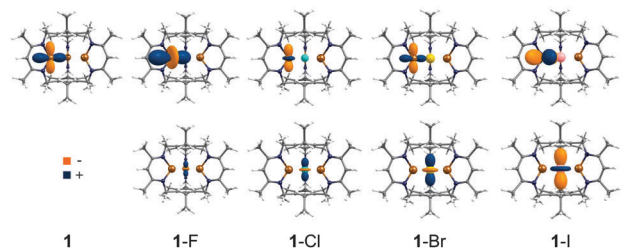

Fig. 3 Graphical representation of copper and guest quadrupole moment tensors.

Table 6 Principal components of the electronic quadrupole tensor of the studied systems, for a representative cooper and guests (Buckinghams)

	Cu				X			
	Θ_{11}	Θ_{22}	Θ_{33}	Θ_{aniso}	Θ_{11}	Θ_{22}	Θ_{33}	Θ_{aniso}
1	−0.412	−0.244	0.656	0.984	—	—	—	—
1-F	−0.482	−0.474	0.957	1.435	−0.087	−0.087	0.173	0.26
1-Cl	0.146	0.056	−0.203	−0.304	−0.108	−0.108	0.216	0.324
1-Br	−0.201	−0.056	0.257	0.386	−0.175	−0.175	0.350	0.525
1-I	−0.351	−0.047	0.398	0.597	0.588	0.588	−1.175	−1.763

The graphical quadrupole moment analysis shows that in **1**, the negative lobe, represented by Θ_{11} and Θ_{22}, is mainly distributed along the Cu–N bonds, whereas the electron deficient region (Θ_{33}) points toward the center of the cavity.

In the first three complexes a match occurs between such a positive lobe and the negative lobe of the halide guest, which is distributed in the same plane of Cu(I) centers. In the iodide system, a different distribution occurs, suggesting that the host cavity size induces iodide to distribute its electronic charge above and below the Cu(I) center plane, leaving an electron deficient region in the center. This new distribution influences the copper generating a local quadrupole distortion in which a negative lobe now points toward the guest electron deficient region, leading to a more effective quadrupole–quadrupole match (*i.e.* negative lobe with positive lobe). Remarkably, in this inclusion system the highest anisotropy value is obtained for the guest species ($\Theta_{aniso} = -1.763$). For the Cu(I) centers, the **1**-F case exhibits the largest anisotropic value at such center driven by its largest Θ_{33} component pointing directly to the F^- guest, suggesting an enhanced interaction due to the short distance (2.109 Å, Table 1).

In addition, the **2**-X series (Fig. S1, ESI†) exhibits the same quadrupole variation as **1**-X, evidencing the low contribution of the aromatic rings in the quadrupole distortion of the binding sites, in agreement to the discussion above. These results are confirmed by the quadrupole moment analysis of the **3**-X series, where the anisotropy values are lower in comparison to those corresponding to the **2**-X series, proving the minor influence of the aromatic rings on the electronic cloud departure, especially in the first three systems. In **3**-I, again the aromatic rings seem to alter the iodide quadrupole moment, but only to a small extent ($\Theta_{aniso} = 0.417$).

Lastly, the spatial distribution of non-covalent interactions has been evaluated according to the Non-covalent Interactions (NCI) analysis,[32,33] which is based on a 2D plot of the reduced density gradient, s, and the electron density $\rho(r)$, where can be expressed as

$$s = \frac{1}{2(3\pi^2)^{1/3}} \frac{\nabla\rho}{\rho^{4/3}}$$

When non-covalent interactions occur, there is a crucial change in s, producing density critical points. Then, an isosurface considering only the values of s associated with the critical points is generated, denoting where noncovalent forces occur. To determine the type of interaction, the second

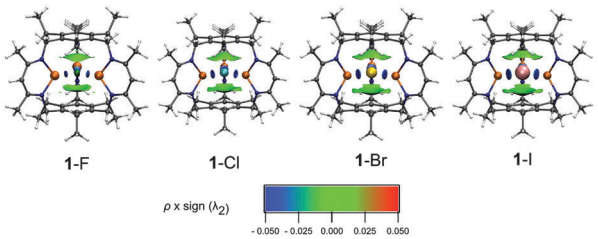

Fig. 4 NCI Analysis for **1**-X (X = F, Cl, Br, I).

eigenvalue of the electronic density Hessian (λ_2) is invoked, where more than weak stabilizing interactions, such as hydrogen bonds, are characterized by $\lambda_2 < 0$, non-bonded interactions such as steric repulsion by $\lambda_2 > 0$, and weak interactions by $\lambda_2 \lesssim 0$. These are denoted by $\lambda_2 < 0$ values over the isosurface, by using a colour scale.

From the NCI analysis carried out for the halide series (**1**-X), considering the scale $-0.05 < \rho < 0.05$, blue regions between the copper centers and the guest species revealing more than weak interactions ($\lambda_2 < 0$) between them (Fig. 4) can be noted. Also green regions corresponding to weak forces ($\lambda_2 \lesssim 0$) between the aromatic rings of the cyclophane cage and the halide ions can be observed, which also have been identified in several systems with anions in close contact with π acidic aromatic ligands.[51] The NCI analysis supports our statement that the guest species are mainly stabilized in the center of the cavity by Cu(I)···X interactions with a minor contribution of π···X forces.

Concluding remarks

We evaluated the preference of the metal-containing cryptand, which exhibits a more stable situation with the hardest guest anion F^- because of the Pauli repulsion term which markedly decreases as the guest becomes smaller allowing the stabilization of contributions to more effectively overcome repulsion forces in the fluoride system. The role of higher order Coulombic terms is evidenced to a major extent in the iodide inclusion system where the softer guest experiences a higher electronic cloud variation, then allowing a different quadrupole distribution in comparison to the rest of the series, leading to a close match with the copper centers.

By exploring the electrostatic contribution in more detail, we found that as the guest becomes softer, the increase of higher order Coulombic terms, such as dipole–dipole, dipole–quadrupole, and quadrupole–quadrupole, acquires more relevance on going from 9.22% to 41.25%. The presence of weak stabilizing interactions between the copper centers and the halide ions is evidenced by the NCI analysis, which can be associated with the spatial distribution of the dipole quadrupole and quadrupole–quadrupole stabilizing interactions occurring between such species.

Interestingly, the study of the metal-based cryptand host reveals the role of higher order Coulombic terms in the overall host–guest interaction, where a hard guest depicts an interaction characterized by ion-multipole forces. In contrast, the soft guest exhibits a large contribution of higher rank terms. Hence, into the analysis of non-covalent interactions according to the HSAB theory, such variation of the contributing terms should be taken into account in the design of novel host–guest species.

Acknowledgements

The authors thank to Centre national de la recherche scientifique (CNRS), FONDECYT Grant 1140358 and PROJECT MILLENNIUM No. RC120001, for financial support.

Notes and references

1 D. G. Graczyk, R. L. Julian and J. W. Taylor, *J. Am. Chem. Soc.*, 1975, **97**, 7382.
2 V. M. Loyola, R. Pizer and R. G. Wilkins, *J. Am. Chem. Soc.*, 1977, **99**, 7185.
3 K. Dabrowa, M. Pawlak, P. Duszewski and J. Jurczak, *Org. Lett.*, 2012, **14**, 6298.
4 G. Alibrandi, V. Amendola, G. Bergamaschi, L. Fabbrizzi and M. Licchelli, *Org. Biomol. Chem.*, 2015, **13**, 3510.
5 G. E. Alliger, P. Müller, L. H. Do, C. C. Cummins and D. G. Nocera, *Inorg. Chem.*, 2011, **50**, 4107.
6 K. E. Krakowiak, X. X. Zhang, J. Bradshaw, C. Y. Zhu and R. M. Izatt, *J. Inclusion Phenom. Mol. Recognit. Chem.*, 1995, **23**, 223.
7 M. Zhang, X. Yan, F. Huang, Z. Niu and H. Gibson, *Acc. Chem. Res.*, 2014, **47**, 1995.
8 D. Landini, A. Maia, F. Montanari and P. Tundo, *J. Am. Chem. Soc.*, 1979, **101**, 2526.
9 R. E. A. Dillon and D. F. Shriver, *Chem. Matter.*, 1999, **11**, 3296.
10 V. Amendola, G. Bergamaschi, M. Boiocchi, R. Alberto and H. Braband, *Chem. Sci.*, 2014, **5**, 1820.
11 G. Mezei, C. M. Zaleski and V. L. Pecoraro, *Chem. Rev.*, 2007, **107**, 4933, and references therein.
12 A.-M. Caminade and J. Majoral, *Chem. Rev.*, 1994, **94**, 1183.
13 G. Di Francesco, A. Gaillard, I. Ghiviriga, K. Abboud and L. Murray, *Inorg. Chem.*, 2014, **53**, 4647.
14 S. O. Kang, J. M. Linares, V. W. Day and K. Bowman-James, *Chem. Soc. Rev.*, 2010, **39**, 3980, and references therein.
15 R. Pearson, *J. Chem. Sci.*, 2005, **117**, 369.
16 R. Pearson, *J. Chem. Educ.*, 1968, **45**, 581.
17 J. W. Steed and J. L. Atwood, *Supramol. Chem.*, Wiley, UK, Second edn, 2009.
18 K. Ariga and T. Kunitake, *Supramolecular Chemistry: Fundamentals and Applications*, Springer, Berlin, 2005.
19 R. J. Doerksen and A. J. Thakkar, *J. Phys. Chem. A*, 1999, **103**, 10009.
20 J. H. Williams, *Acc. Chem. Res.*, 1993, **26**, 593.
21 P. Hobza and K. Müller-Dethlefs, *Non-covalent Interactions, Theory and Experiment*, Royal Society of Chemistry, Cambridge, 2010.

22 M. R. Jackson, R. Beahm, S. Duvvuru, C. Narasimhan, J. Wu, H.-N. Wang, V. M. Philip, R. J. Hinde and E. E. Howell, *J. Phys. Chem. B*, 2007, **111**, 8242.
23 K. Shimizu, M. F. Costa Gomes, A. A. H. Pádua, L. P. N. Rebelo and J. N. C. Lopes, *J. Phys. Chem. B*, 2009, **113**, 9894.
24 T. Shimizu, J. Jung, H. Imada and Y. Kim, *Angew. Chem., Int. Ed.*, 2014, **53**, 13729.
25 M. Ponce-Vargas and A. Muñoz-Castro, *Phys. Chem. Chem. Phys.*, 2014, **16**, 13103.
26 M. Ponce-Vargas and A. Muñoz-Castro, *J. Phys. Chem. C*, 2014, **118**, 28244.
27 K. Moroukuma, *J. Chem. Phys.*, 1971, **55**, 1236.
28 K. Kitaura and K. Morokuma, *Int. J. Quantum Chem.*, 1976, **10**, 325.
29 S. Grimme, *J. Comput. Chem.*, 2004, **25**, 1463.
30 S. Grimme, *WIREs Comput. Mol. Sci.*, 2011, **1**, 211.
31 M. Swart, P. Van Duijnen and J. G. Snidjers, *J. Comput. Chem.*, 2001, **22**, 79.
32 E. R. Johnson, S. Keinan, P. Mori-Sanchez, J. Contreras-García, A. J. Cohen and W. Yang, *J. Am. Chem. Soc.*, 2010, **132**, 6498.
33 J. Contreras-García, E. R. Johnson, S. Keinan, R. Chaudret, J. Piquemal, D. N. Beratan and W. Yang, *J. Chem. Theory Comput.*, 2011, **7**, 625.
34 R. Parr and W. Yang, *Density Functional Theory of Atoms and Molecules*, Oxford University Press, New York, 1989.
35 Amsterdam Density Functional (ADF) code. Release 2010, Vrije Universiteit, Amsterdam, Netherlands, 2011.
36 J. Tao, J. P. Perdew, V. N. Staroverov and G. E. Scuseria, *Phys. Rev. Lett.*, 2003, **91**, 146401.
37 M. P. Johansson and M. Swart, *Phys. Chem. Chem. Phys.*, 2013, **15**, 11543.
38 V. N. Staroverov and G. E. Scuseria, *J. Chem. Phys.*, 2003, **119**, 12129.
39 Y. Zhao and D. G. Truhlar, *J. Chem. Phys.*, 2006, **124**, 224105.
40 J. Tao, S. Tretiak and J. Zhu, *J. Chem. Phys.*, 2008, **128**, 084110.
41 L. Verluis and T. Ziegler, *J. Chem. Phys.*, 1988, **88**, 322.
42 E. Zurek, C. J. Pickard and J. Autschbach, *J. Phys. Chem. C*, 2008, **112**, 11744.
43 G. A. Zhurko, http://www.chemcraftprog.com.
44 W. Humphrey, A. Dalke and K. Schulten, *J. Mol. Graphics*, 1996, **14**, 33.
45 M. Von Hopffgarten and G. Frenking, *WIREs Comput. Mol. Sci.*, 2012, **2**, 43.
46 J.-Y. Liang and W. Lipscomb, *J. Phys. Chem.*, 1986, **90**, 4246.
47 P. Su and H. Li, *J. Chem. Phys.*, 2009, **131**, 014102.
48 S. F. Boys and F. Bernardi, *Mol. Phys.*, 1970, **19**, 553.
49 R. D. Shannon, *Acta Crystallogr., Sect. A: Cryst. Phys., Diffr., Theor. Gen. Crystallogr.*, 1976, **32**, 751.
50 U. Haberlen, *U. Advances in Magnetic Resonance*, suppl. 1, Academic Press, New York, London, 1976.
51 H. T. Chifotides and K. R. Dunbar, *Acc. Chem. Res.*, 2013, **46**, 894.